Available online at www.sciencedirect.com
SCIENCE DIRECT
Journal of Power Sources 157 (2006) 56–63
JOURNAL OF POWER SOURCES
www.elsevier.com/locate/jpowsour

# Studies on Co-based catalysts supported on modified carbon substrates for PEMFC cathodes

Nalini P. Subramanian [a], Swaminatha P. Kumaraguru [a], Hector Colon-Mercado [a], Hansung Kim [c], Branko N. Popov [a,*], Timothy Black [b], Donna A. Chen [b]

[a] *Department of Chemical Engineering, University of South Carolina, Columbia, SC 29208, USA*
[b] *Department of Chemistry and Biochemistry, University of South Carolina, Columbia, SC 29208, USA*
[c] *Department of Chemical Engineering Yonsei University, Seoul, South Korea*

Received 18 April 2005; received in revised form 9 June 2005; accepted 10 July 2005
Available online 26 August 2005

**Abstract**

Cobalt based non-precious metal catalysts were prepared by supporting cobalt-ethylene diamine complex on carbon followed by a heat treatment at elevated temperatures (800 °C). Surface oxygen groups on carbon were introduced with $HNO_3$ oxidation. Co catalysts supported on oxidized carbon showed improved activity and selectivity towards four-electron reduction of molecular oxygen. Quinone groups introduced by nitric acid treatment, in addition to increasing the dispersion of the chelate complexes, play a role in forming the active site for oxygen reduction.


*Keywords:* PEM fuel cells; Oxygen reduction; Non-noble metal catalyst; Electrocatalysis; Carbon activation

## 1. Introduction

In recent years, there has been considerable interest in the development of non-precious metal catalysts [1–6] as Pt substitutes for cathodes in polymer electrolyte membrane fuel cells (PEMFCs). Prominent among them are macrocycle-based metal-containing porphyrin systems [1,2], chevrel phase type compounds (e.g., $Mo_4Ru_2Se_8$) [3] and other transition metal chalcogenides [4,5]. Côté et al. [6] demonstrated activity for transition metals supported on carbon followed by heat treatment in $NH_3$ atmosphere. Alternatively, heat-treated Co-chelate complexes dispersed on carbon showed considerable activity for oxygen reduction in acidic media [7]. Heat treatment of macrocycles in an inert atmosphere enhanced the catalytic activity and stability [8]. Generation of an $M–N_4$ type moiety with heat treatment at elevated temperatures is widely known to act as the catalytic site for the oxygen reduction reaction [9]. Only a few studies are available on the role of carbon support and surface functional groups in the formation of the catalytic site. However, for Pt catalysts, dispersion and utilization of the catalysts were found to strongly depend on the surface functionalities [10–14] and pore size characteristics [15]. Jaouen et al. [16] showed that pre-treatment of carbon resulted in an improvement in the performance of Fe-based non-precious metal catalysts to oxygen reduction reaction (ORR). According to the studies of Ehrburger et al. [17] on iron phthalocyanine (FePC), oxygen surface complexes on the edge carbon atoms anchor the FePC particles and aid in improved dispersion of these particles. Gouérec et al. [18] studied the activity and stability of cobalt tetraazaannulene (CoTAA) on two different carbon supports varying in the amount of surface oxygen complexes, and concluded that strong interactions between the metal complex and the carbon support are established via the surface oxygen complexes thus increasing the sintering resistance of these particles. In addition, chalcogen group elements such as O [18], S [19] and Se [20] have been shown to act as promoters for oxygen reduction reaction. The objective of this work is to study the performance of cobalt-chelate electrocatalysts effected by

* Corresponding author. Tel.: +1 803 777 7314.
*E-mail address:* popov@engr.sc.edu (B.N. Popov).

0378-7753/$ – see front matter © 2005 Elsevier B.V. All rights reserved.
doi:10.1016/j.jpowsour.2005.07.031

characteristics of carbon: its surface oxygen groups, specific surface area and pore size distribution.

## 2. Experimental

### 2.1. Catalyst preparation

Commercially available carbon blacks, namely Ketjen Black EC 300 J, Vulcan XC-72 and Black Pearl 2000, were pre-washed with 6 M HCl to dematerialize the carbon of any metal impurities [21]. This carbon was then washed in distilled water to remove any chloride impurities. The pre-washed carbon was subjected to oxidation in 70% $HNO_3$ for 7 h under reflux and then washed in distilled water, followed by drying in an oven at 75 °C to obtain oxidized carbon. For brevity, as-received Ketjen Black EC 300 J, Vulcan XC-72 and Black Pearl 2000 are denoted as K, V and B; HCl treated carbons as K1, V1 and B1; $HNO_3$ treated carbons as K2, V2 and B2. Both oxidized carbon (e.g., K2) and un-oxidized carbon (e.g., K1) were loaded with Co-chelate complex (denoted as CoEDA). The cobalt ethylene diamine (CoEDA) chelate gives rise to the simplest $MN_4$ structure among the chelates studied [22]. This complex was synthesized by adding stoichiometric amounts of ethylene diamine to cobalt nitrate under stirring conditions in ethanol [7]. The cobalt complex synthesized was dispersed on carbon in ethanol solvent under reflux conditions for 4 h. The loading of Co with respect to carbon is 20%. This loading was kept constant for all the samples synthesized with Co. The carbon loaded with the cobalt complex was dried in a rotary evaporator at 80 °C under vacuum. This dried sample was subjected to heat treatment at 800 °C in Ar atmosphere for 1 h. For comparison studies and to elucidate the effect of cobalt, carbon loaded with metal-free ethylene diamine was prepared under similar conditions and denoted as K1-EDA(HT) and K2-EDA(HT) on un-oxidized and oxidized carbon supports, respectively.

### 2.2. Electrochemical characterization

Electrochemical characterizations were performed in a single-compartment, three-electrode cell. A rotating ring disk electrode from Pine Instruments with a glassy carbon disk (5 mm o.d.) and Pt ring (5.52 mm i.d. and 7.16 o.d.) was used as the working electrode. Platinum wire was used as the counter electrode. A standard $Hg/HgSO_4$ electrode was used as the reference electrode. The potentials presented in this study are referred with respect to standard hydrogen electrode (SHE). The electrocatalyst was applied to the disk electrode in the form of an ink. Eight milligrams of the prepared electrocatalyst was suspended in 1 ml of isopropyl alcohol and ultrasonically blended for 10 min. Fifteen microliters of this suspension is applied on the disk electrode in steps of 5 μl, with drying after each addition. Five microliters of Nafion solution (1:10:10 :: 5 wt% Nafion:water:isopropyl alcohol) was added on top of the former film. 0.5 M $H_2SO_4$ was used as the electrolyte in all studies. Initially, the solution was purged with nitrogen and cyclic voltammograms (CVs) were recorded by scanning the disk potential from 1.04 V to 0.04 V versus SHE at a scan rate of 5 mV $s^{-1}$. CVs recorded at 5 mV $s^{-1}$ in nitrogen atmosphere were used to obtain the background capacitive currents. For all electrochemical measurements, the ring potential was maintained at 1.2 V versus SHE to oxidize any peroxide produced. Before the measurement of oxygen reduction currents, the electrolyte solution was purged with oxygen for 15 min. A CV was recorded in this oxygen saturated electrolyte, followed by linear sweep voltammograms at different rotation rates of the RRDE for disk potentials from 1.04 V to 0.04 V versus SHE at a scan rate of 5 mV $s^{-1}$. All measurements were taken using a bipotentiostat (Model AFRDE from Pine Instruments).

### 2.3. Physical and surface characterization

The particle size of the catalyst was determined using transmission electron microscopy (TEM, Hitachi H-8000 model). Surface analysis of the catalyst was performed by X-ray photoelectron spectroscopy (XPS). Experiments were carried out in a stainless steel ultrahigh vacuum chamber (Leybold) with a base pressure $\leq 1 \times 10^{-9}$ Torr which has been described in more detail elsewhere [23]. The chamber is equipped with a single-channel hemispherical energy analyzer (Leybold LA10) and Al Kα anode X-ray source (1486.6 eV), as well as a load lock chamber for fast sample introduction. The powdered samples were loaded onto conductive, double-sided silver tape (Structure Probe Inc.) for the XPS experiments. For each sample, the Co(2p), C(1s), N(1s) and O(1s) regions were collected with a step size of 0.05 eV, dwell time of 0.2 s and pass energy of 50 eV, and were averaged over 10 scans. Lower resolution survey scans were collected with a step size of 1.0 eV, dwell time of 0.2 s and pass energy of 50 eV, and were averaged over four scans.

## 3. Results and discussion

### 3.1. Significance of surface oxygen groups

The un-oxidized K1 and oxidized K2 bare carbon supports were tested initially for their activity for oxygen reduction. Fig. 1a illustrates a typical polarization curve obtained on a rotating disk electrode for electrochemical reduction of molecular oxygen in 0.5 M $H_2SO_4$. It can be seen that un-oxidized carbon K1 has negligible activity to oxygen reduction. However, with the introduction of surface oxygen groups by $HNO_3$ treatment, the activity of the carbon increases. Oxidized carbon K2, shows about 100 mV less activation overpotential for oxygen reduction reaction compared to K1. Electrochemical analysis indicates that car-

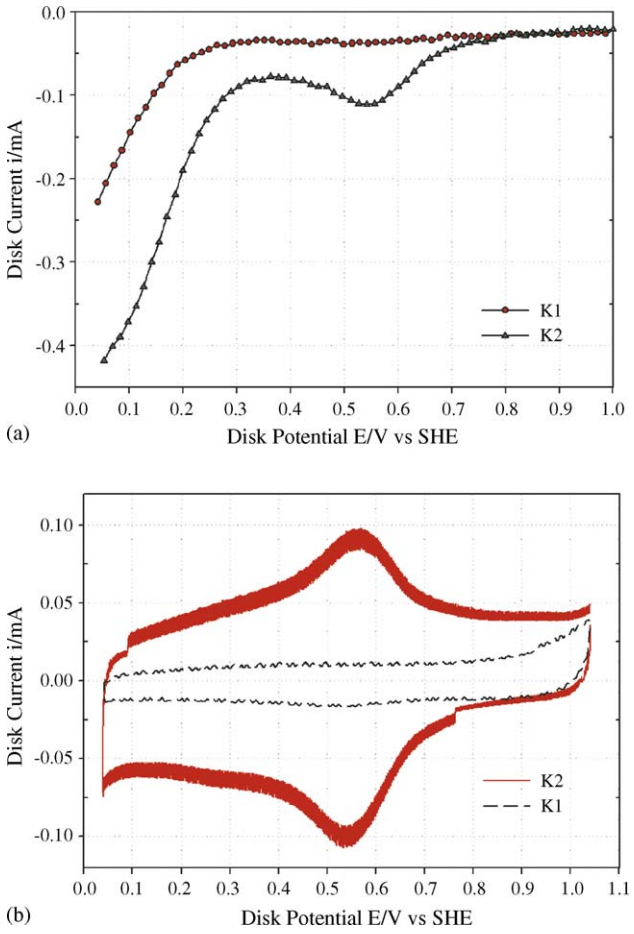


Fig. 1. (a) Polarization curve of K1 and K2 in 0.5 M $H_2SO_4$ solution saturated with $O_2$. Scan rate 5 mV $s^{-1}$ and rotation rate 900 rpm. (b) Typical cyclic voltammograms of K1 and K2 in 0.5 M $H_2SO_4$ saturated with $N_2$. Scan rate 5 mV $s^{-1}$ and rotation rate 0 rpm.

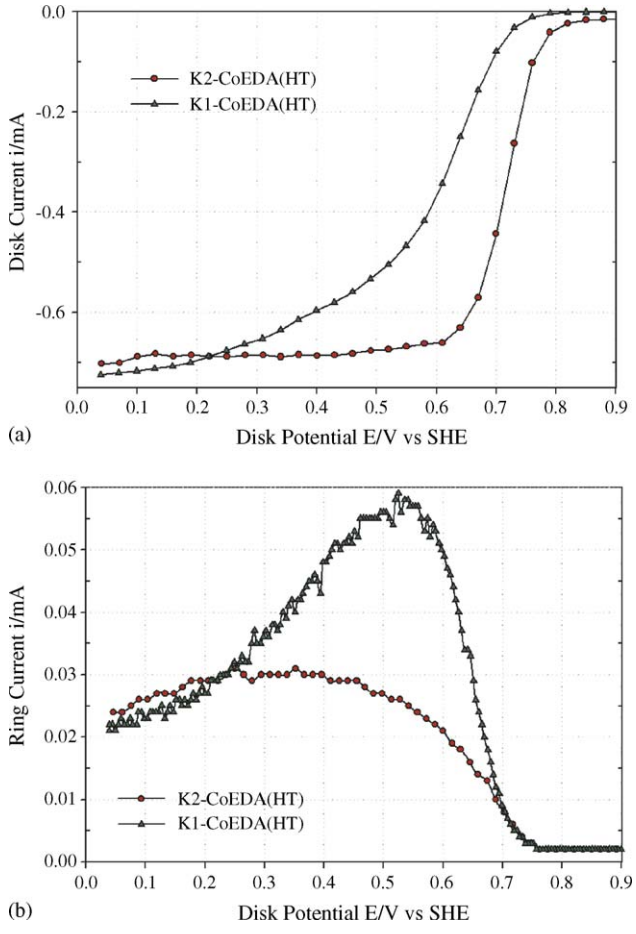


Fig. 2. Polarization curve of heat treated CoEDA samples on oxidized and un-oxidized carbons for oxygen reduction in 0.5 M $H_2SO_4$ solution saturated with $O_2$. (a) Disk currents and (b) ring currents. Scan rate 5 mV $s^{-1}$ and rotation rate 900 rpm.

bon oxidation in nitric acid introduces quinone type oxygen groups on the carbon surface [24,25]. The nature of the surface functional groups generated with $HNO_3$ treatment was studied using cyclic voltammograms. The CVs were performed on un-oxidized (K1) and oxidized (K2) carbon supports. Fig. 1b illustrates the cyclic voltammograms obtained for carbons K1 and K2 in 0.5 M $H_2SO_4$ saturated with $N_2$. The un-oxidized carbon (K1) does not exhibit any characteristic peak. $HNO_3$ oxidized carbon (K2) exhibits well-defined redox peaks at 0.55 V versus SHE. These characteristic peaks are associated with the quinone–hydroquinone redox couple [24]. The effect of oxidation on the dispersion and the activity of cobalt-chelate complexes was studied by testing the samples of heat treated CoEDA on oxidized carbon K2 and on un-oxidized carbon K1. The results are shown in Fig. 2. The electrocatalyst K2-CoEDA(HT) showed better activity than K1-CoEDA(HT). The catalyst supported on un-oxidized carbon exhibits activation overpotential of 470 mV oxygen reduction. The diffusion-limited plateau of the polarization curve for K1-CoEDA(HT), shown in Fig. 2a, is not well defined as is usually observed with the Pt catalysts. The model proposed by Jiang and Anson [26] shows that the plateau is more inclined when the distribution of active sites is less uniform and the reaction is slower. However, with the use of $HNO_3$ treated oxidized carbon, activity towards oxygen reduction increases. A single steep reduction wave with a well-developed limiting plateau similar to that of Pt catalysts is observed. The activation overpotential for oxygen reduction on K2-CoEDA(HT) decreases by 60 mV compared to K1-CoEDA(HT). Fig. 2b gives the ring currents as a function of the disk potential of the two catalysts. The ring currents on K2-CoEDA(HT) are less than on K1-CoEDA(HT). This suggests that the selectivity of the catalyst to the four-electron reduction of oxygen to water is increased on oxidized carbon. Another interesting feature is the shape of the ring currents on both the samples. The ring current is a function of the potential and goes through a maximum. Oxygen reduction reaction is potential-dependent. Potential-dependent selectivity of the oxygen reduction reaction on iron porphyrin has been studied previously [27]. The shape of the ring currents of iron porphyrin catalysts studied in that literature reference are similar to the ones obtained in cobalt-chelate catalysts in our work.

Table 1
Average particle size and standard deviation of catalysts analyzed in TEM

| Sample | Average particle size (nm) | Standard deviation (nm) |
|---|---|---|
| K1-CoEDA(HT) | 23.7 | 24.5 |
| K2-CoEDA(HT) | 9.5 | 3.8 |
| B2-CoEDA(HT) | 12.5 | 8.4 |
| V2-CoEDA(HT) | 40 | 12 |

$O_2$ reduction follows the general scheme shown below in Eq. (1).

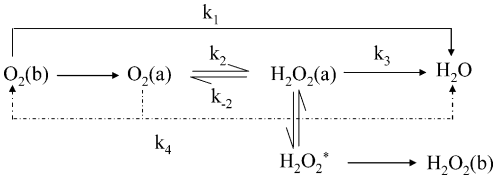


(1)

Indices a, * and b indicate adsorbed, in the vicinity of the disk electrode and in the bulk, respectively. At high potentials $k_1/k_2$ is constant with $k_1 > k_2$ indicating a direct reduction of oxygen to water than the two-electron reduction to peroxide. At intermediate potentials $k_1/k_2$ ratio is falling indicating an increase in the two-electron reduction to peroxide. At lower potentials $k_1/k_2$ becomes lower than 1. However, $k_3$ increases resulting in a further reduction of peroxide to water before it escapes into the solution.

Nitrogen fixation on carbon from nitrogen containing precursors increase with the amount of oxygen surface groups [28,29], with one atom of nitrogen being added for every oxygen atom in the quinone structure. Such quinone groups form acidic sites on the carbon surface which favor the absorption of the basic CoEDA complex [30]. This phenomenon results in an increase in dispersion of the catalyst. Fig. 3a and b shows the TEM images of heat treated CoEDA samples supported on oxidized carbon and un-oxidized carbon. The average particle size along with the standard deviation is given in Table 1. The average particle size of the catalyst supported on K1 is 23.7 nm while the particle size for the catalyst loaded on K2 support is 9.5 nm. Thus, the surface quinone groups cause a better dispersion of the CoEDA complex. By increasing the number of oxygen groups on the carbon support, the dispersion of the catalysts, as well as their ultimate performance, is increased.

Table 2
Commercial carbons used and their surface areas

| Carbon | Area ($m^2\ g^{-1}$) | Micropores ($m^2\ g^{-1}$) | Mesopores ($m^2\ g^{-1}$) |
|---|---|---|---|
| Ketjen Black | 886 | 55 | 680 |
| Vulcan XC-72 | 254 | 118 | 100 |
| Black Pearl 2000 | 1500 | 720 | 540 |

### 3.2. Effect of carbon surface area and pore size distribution

The effect of surface area and pore size distribution of the carbon support on the activity of heat treated CoEDA catalysts was studied using three commercial carbons, namely Ketjen Black EC 300 J, Vulcan XC-72 and Black Pearl 2000.

The total specific surface areas, mesopore areas and micropore areas of the as-received carbon supports are summarized in Table 2. The carbon supports were pre-washed in HCl and oxidized with $HNO_3$ as explained in Section 2. The oxidation of carbon results only in a slight decrease in surface area and hence will not alter the distribution of the pores to a large extent (and hence the proportion of mesopores) [31]. Thus, the comparisons of the carbon surface area and the pore size distribution are based on the values for as-received carbons (K, V and B). Fig. 4a shows the cyclic voltammograms of the oxidized carbons K2, B2 and V2 in nitrogen atmosphere. The redox peaks of quinone–hydroquinone couple are well pronounced in B2 and K2 compared to V2. Nitric acid oxidation attacks the relatively weak sites of the carbon structure which occurs at the edges of the basal planes [32]. However, only the mesopores with pore diameters of 2–50 nm are accessible to nitric acid oxidation since they possess a combination of high surface area and large pore diameter [33]. The area inside the micropores with a diameter smaller than 2 nm is inaccessible for nitric acid oxidation. Hence, higher surface area does

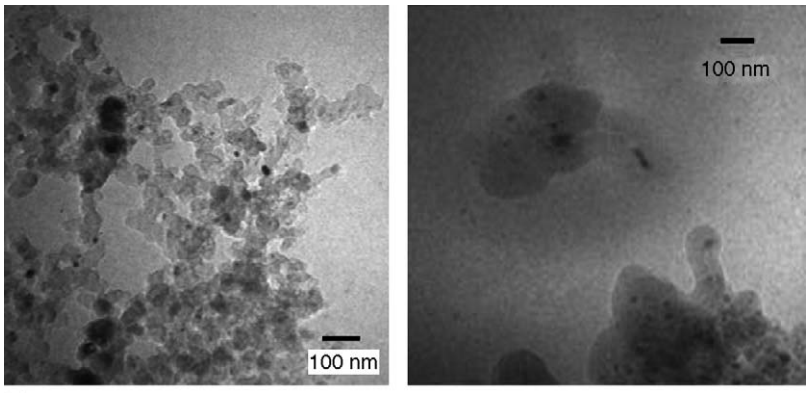


Fig. 3. TEM image of (a) K1-CoEDA(HT) and (b) K2-CoEDA(HT).

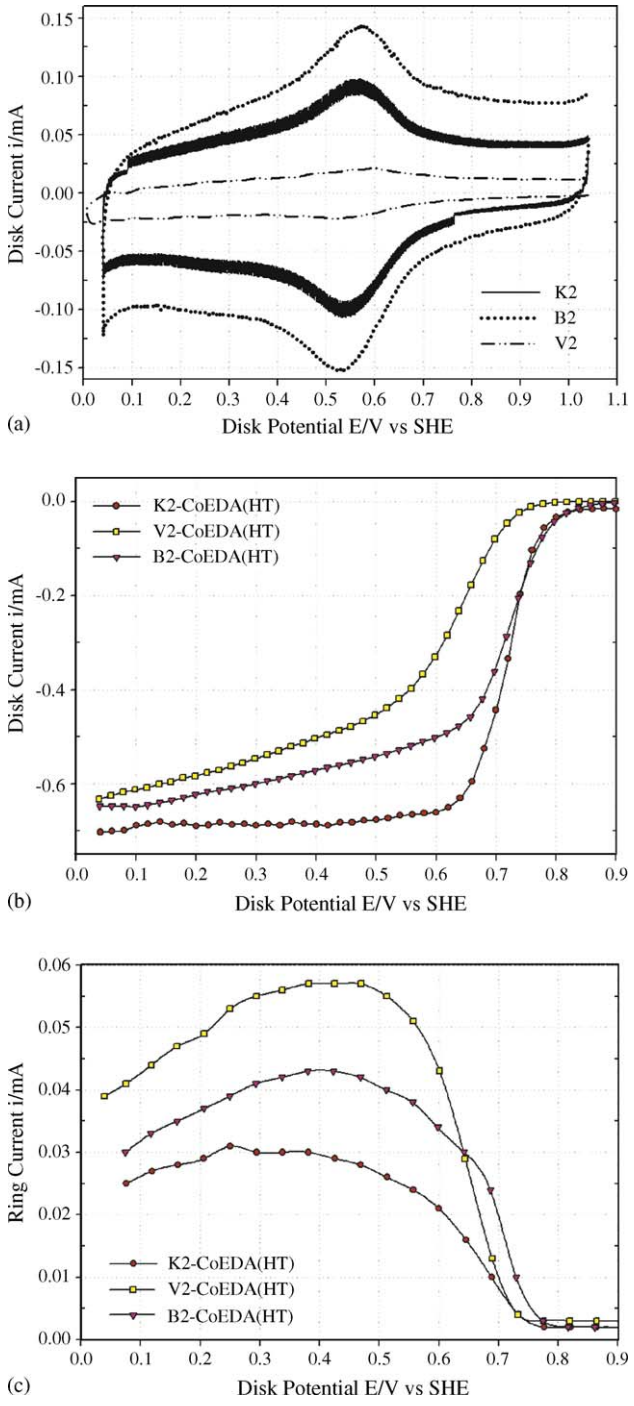


Fig. 4. (a) Typical cyclic voltammograms of oxidized carbon K2, B2 and V2 in 0.5 M $H_2SO_4$ saturated with $N_2$. Scan rate 5 mV $s^{-1}$, rotation rate 0 rpm and polarization curves of heat treated CoEDA samples supported on K2, B2 and V2 in 0.5 M $H_2SO_4$ solution saturated with oxygen. (b) Disk currents and (c) ring currents. Scan rate 5 mV $s^{-1}$ and rotation rate 900 rpm.

not necessarily mean higher number of such oxidation-prone sites. As shown in Table 2, the surface area of Black Pearl 2000 is higher than that of Ketjen Black EC 300 J followed by Vulcan XC-72. The increase in the surface area in Black Pearl 2000 compared to Ketjen Black EC 300 J results from the increase of the area inside the micropores (720 $m^2$ $g^{-1}$). Since, as discussed above, the micropores are not accessible for nitric acid oxidation, the amount of quinone groups in acid treated B2 does not increase when compared with that of K2.

Fig. 4b shows polarization curves in 0.5 M $H_2SO_4$ of CoEDA complex loaded on the three oxidized carbons and heat treated to obtain the catalysts K2-CoEDA(HT), B2-CoEDA(HT) and V2-CoEDA(HT). The activity of the heat treated catalyst decreases as follows on the oxidized carbons: K2 > B2 > V2. Also, a comparison of the ring currents as shown in Fig. 4c indicates that the ring currents decrease with the increase of the amount of quinone groups as given by the CVs in $N_2$ in Fig. 4a. Also, the shape of the ring currents is similar to those in Fig. 2b. Thus, the higher the amount of quinone groups, the higher the selectivity to the four-electron reduction of oxygen to water. The catalyst performance increases with increased dispersion of the catalyst which increases with the amount of quinone groups on carbon surface.

TEM images presented in Figs. 3b and 5a and b provide supporting evidence that the average particle size of cobalt in K2-CoEDA(HT) is 9.5 nm compared to 12.5 nm for B2-CoEDA(HT) and 40 nm for V2-CoEDA(HT). The bigger particle size is due to a decrease of quinone groups resulting from a decreased mesopore area.

The charge under the peaks of the nitrogen CVs corresponding to quinone/hydroquinone couple was calculated and it turns out to be that, among the oxidized carbons, Ketjen has slightly higher charge (after background subtraction). The charges under the peaks are 0.00039053 C, 0.0020854 C, 0.002029 C and 0.0 C for V2, K2, B2 and K1, respectively. The lower particle size in the case of catalysts loaded on K2 compared to that on V2 and B2 is due to the higher peak area observed on K2. However, the very small difference in the calculated charges between Black Pearl and Ketjen does not warrant this conclusion. Higher mesopore area in Ketjen itself can be another reason why CoEDA on Ketjen shows a smaller particle size. This can be further substantiated by comparing the particle size of CoEDA on oxidized Vulcan XC-72, V2 (with lower mesopore area) to that on un-oxidized Ketjen Black EC 300 J, K1 (with higher mesopore area). The average particle size of V2-CoEDA is 40 nm and that of K1-CoEDA is 23.7 nm. Thus, both the number of the oxygen groups and the mesoporous area contribute to the increase in the dispersion of the catalyst.

### 3.3. Role of O, N and Co on active site

Fig. 6a shows the polarization curves for K2-EDA(HT) and K2-CoEDA(HT) catalysts on a disk electrode in 0.5 M $H_2SO_4$ saturated with oxygen. The performance of K2-CoEDA(HT) and K2-EDA(HT) catalysts is compared with the E-TEK 19.1% Pt/C-14 $\mu g_{Pt}$ $cm^{-2}$. The ring currents were measured to estimate the amount of hydrogen peroxide produced during oxygen reduction. In addition to the increase in dispersion of the CoEDA, the surface oxygen group appears

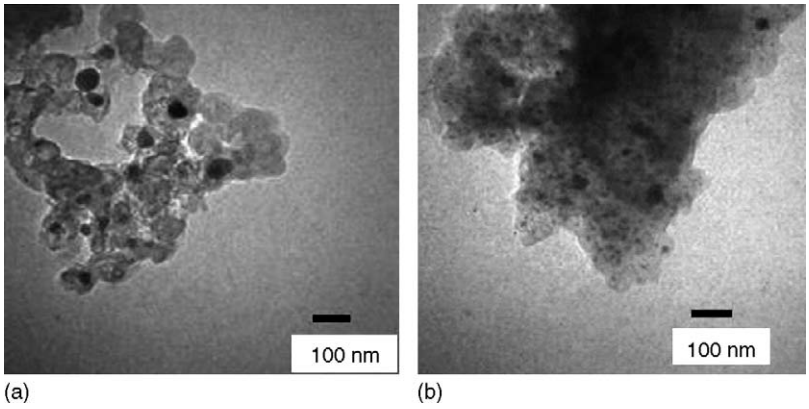


Fig. 5. TEM image of (a) V2-CoEDA(HT) and (b) B2-CoEDA(HT).

to play an important role in the generation of active sites for oxygen reduction, as shown by the polarization curves in Fig. 1a. Further introduction of nitrogen groups, by ethylene diamine adsorption on K2 followed by heat treatment, decreases the activation overpotential towards oxygen reduction by 300 mV. With the incorporation of cobalt in the catalyst, a drastic increase in activity towards oxygen reduction is observed. The on-set potential for oxygen reduction is as high as +820 mV versus SHE. The catalyst shows less than 100 mV higher overpotential for oxygen reduction in comparison to E-TEK 19.1% Pt/C catalyst. The single steep reduction wave with a well-defined diffusion-limited plateau indicates the improved kinetics of the K2-CoEDA(HT) catalyst. Fig. 6b gives the ring currents of the catalysts whose disk currents are given in Fig. 6a. The ring currents were measured to estimate the amount of hydrogen peroxide produced during oxygen reduction. The ring current for K2-EDA(HT) is higher illustrating the large quantity of hydrogen peroxide generated. After addition of Co, the ring current decreases drastically indicating a decrease of the amount of hydrogen peroxide produced. The number of electrons transferred ($n$) and the percentage of peroxide produced ($\%H_2O_2$) can be determined by the following equations [34]:

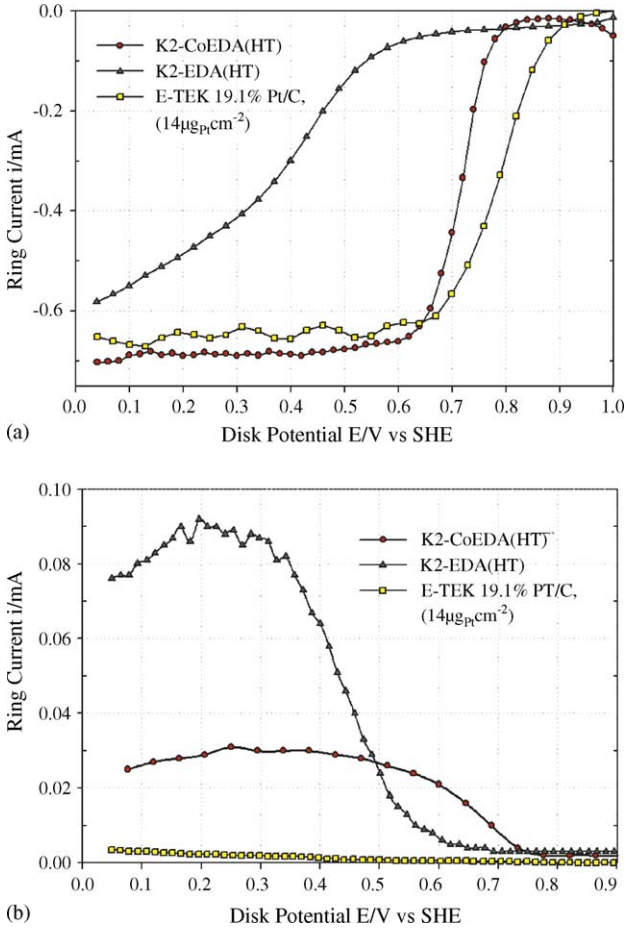


Fig. 6. Polarization curves for K2-EDA(HT) and K2-CoEDA(HT) samples compared to that of commercial E-TEK 20% Pt/C catalysts in 0.5 M $H_2SO_4$ solution saturated with oxygen. (a) Disk currents and (b) ring currents. Disk potential scanned at 5 mV $s^{-1}$ scan rate and rotation rate 900 rpm.

$$n = \frac{4I_D}{I_D + I_R/N} \quad (2)$$

$$\%H_2O_2 = \frac{100(4-n)}{2} \quad (3)$$

where $N$, $I_D$ and $I_R$ are the collection efficiency, disk current and ring current, respectively. We assumed the collection efficiency to be constant at a theoretical value of 0.39 for all the catalysts studied. Fig. 7a and b gives $n$ and $\%H_2O_2$ of the three catalysts K2-EDA(HT), K2-CoEDA(HT) and commercial E-TEK 19.1% Pt/C-14 $\mu g_{Pt}\,cm^{-2}$. It is clearly seen that with Co addition the number of electrons transferred during the oxygen reduction reaction is more than 3.6, and the amount of peroxide produced is less than 20% for most of the potential range examined. Thus, with the addition of the transition metal, the selectivity to the four-electron reduction of oxygen is increased.

### 3.4. XPS measurements

XPS measurements were carried out to examine the changes in surface chemical states due to chemical and heat treatments. An attempt was also made to identify the active

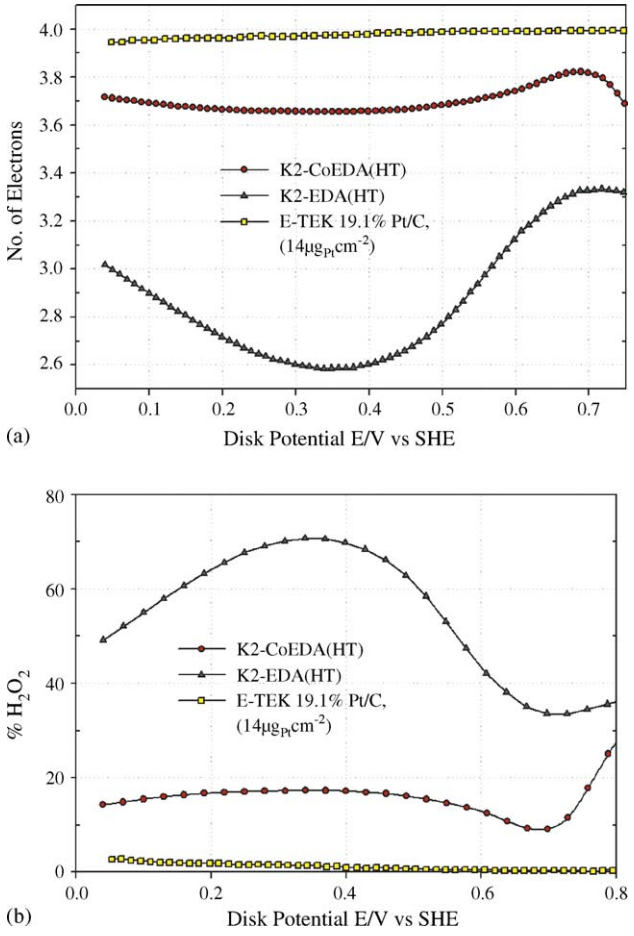


Fig. 7. (a) Number of electrons and (b) percentage peroxide produced calculated from Eqs. (1) and (2) for the catalysts compared in Fig. 6.

surface sites. Samples K1, K2, K1-CoEDA, K2-CoEDA, K1-CoEDA(HT) and K2-CoEDA(HT) were analyzed. Fig. 8a shows the Co($2p_{3/2}$) spectra for the samples K1-CoEDA, K2-CoEDA, K1-CoEDA(HT) and K2-CoEDA(HT). For as-prepared samples, the Co($2p_{3/2}$) peak has a binding energy of approximately 782 eV, which is attributed to Co in a high oxidation state; metallic Co has a binding energy of 777.9 eV, while CoO and $Co_2O_3$ have binding energies of 780 eV and 779.4 eV, respectively [35]. After the heat treatment, the shift in the Co($2p_{3/2}$) peaks to lower binding energies indicates that Co becomes more reduced during this process. The loss of Co signal after heating is consistent with previous reports in the literature indicating that the Co becomes encapsulated with carbon upon heating [36].

Fig. 8b shows the XPS spectra for the N(1s) region for the as-prepared and heat treated samples on various carbon supports. As expected, no nitrogen was detected on the carbon supports before exposure to CoEDA. The presence of nitrogen on the carbon supports was initially detected following treatment with CoEDA, but the intensity of the nitrogen signal decreased almost to zero after the heat treatment, and the shift to lower binding energies indicates a reduction in the nitrogen species.

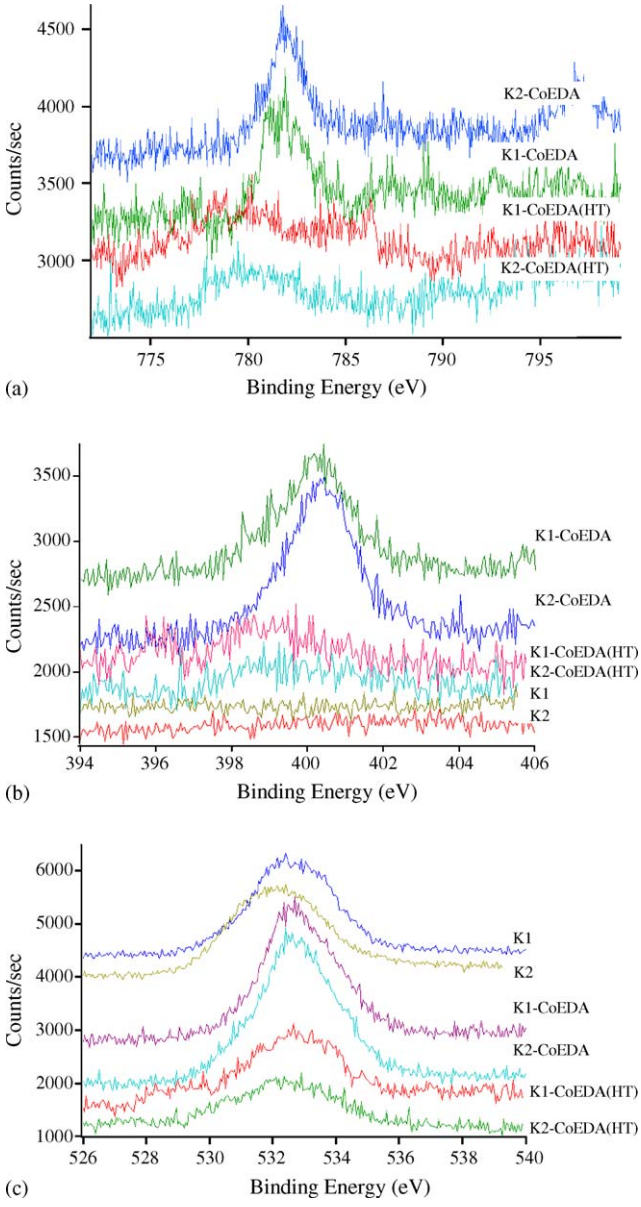


Fig. 8. XPS spectra in (a) Co(2p), (b) N(1s) and (c) O(1s) regions of the samples K1, K2, K1-CoEDA, K2-CoEDA, K1-CoEDA(HT) and K2-CoEDA(HT).

The O(1s) spectra in Fig. 8c show that $HNO_3$ treatment does not substantially increase the amount of surface oxygen on the carbon support. However the nature of the oxygen species is slightly different as demonstrated by the shift in O(1s) binding energies between the spectra for K1 and K2. This is consistent with the electrochemical results where quinone type groups were observed on K2 and not in K1. On both supports, treatment with CoEDA introduces more surface oxygen with higher binding energies. Subsequent heating to 800 °C removes approximately 50–70% of the surface oxygen from the carbon supports and this loss of surface oxygen is consistent with the decrease in oxidation state for the cobalt. Similar to the supports K1 and K2, catalysts K1-CoEDA(HT) and K2-CoEDA(HT) show a slight difference

in O(1s) binding energy, probably due to the presence and absence of quinone groups in K2 and K1, respectively, as observed by the cyclic voltammograms in Fig. 1b.

Regarding the C(1s) region (data not shown), the K1 and K2 supports exhibit similar spectra with a main peak at ∼284.3 eV, a binding energy that has been observed for a number of other carbon supports such as Norit SX Ultra [18,37] and Vulcan SC-72R [36]. The addition of CoEDA results in a peak shift to higher binding energies (285–285.5 eV) due to the presence of carbon in the ethylene diamine complex. However, after heating the CoEDA-treated samples, the resulting spectra are again similar to that of the K1 and K2 supports.

In summary, chemical nature and concentrations of cobalt, nitrogen and oxygen species observed on the two carbon supports are similar to each other before and after treatment with CoEDA, as well as after heating. On both supports, the heat treatment decreases the surface concentration of cobalt, nitrogen and oxygen, and this could be attributed to diffusion of these species into the carbon support [35] or desorption of gaseous nitrogen and oxygen-containing species during heating. Furthermore, the cobalt becomes more reduced upon heating. Thus, a reduced cobalt species (closer to the metallic state) and quinone groups contribute to the observed electrochemical activity.

## 4. Conclusion

Electrochemical techniques were used to characterize the performance of CoEDA catalyst supported on various carbon supports. The influence of oxygen surface groups, surface area and pore size distribution on the catalyst activity has been investigated. Nitric acid treatment introduces quinone groups on the surface of carbon. The quinone groups favor absorption of amines, leading to an increase in dispersion of the cobalt-chelate catalyst, and hence its activity towards ORR. The amount of quinone group increases with the mesoporous area which causes the K2-CoEDA(HT) catalyst to have the highest activity. Introduction of cobalt increases the catalytic activity and favors oxygen reduction via four-electron process. In addition to increasing the dispersion of the catalyst, the presence of quinone oxygen groups enhances the formation of catalytic centers on the carbon support.

## Acknowledgement

Financial support by Department of Energy (DOE) is gratefully acknowledged.

## References

[1] S.Lj. Gojković, S. Gupta, R.F. Savinell, J. Electroanal. Chem. 462 (1999) 63–72.
[2] G. Faubert, R. Côté, D. Guay, J.-P. Dodelet, G. Denes, P. Bertrand, Electrochim. Acta 43 (1998) 341–353.
[3] F.J. Rodríguez, P.J. Sebastian, O. Solorza, R. Pérez, Int. J. Hydrogen Energy 23 (1998) 1031–1035.
[4] N. Alonso-Vante, B. Schubert, H. Tributsch, Mater. Chem. Phys. 22 (1989) 281–307.
[5] N. Alonso-Vante, H. Tributsch, Nature 323 (1986) 431–432.
[6] R. Côté, G. Lalande, G. Faubert, D. Guay, J.P. Dodelet, G. Dénès, J. New Mater. Electrochem. Syst. 1 (1998) 7–16.
[7] V. Birss, A. Sirk, US Patent 0228972 A1 (2003).
[8] P. Gouréc, M. Savy, Electrochim. Acta 44 (1999) 2653–2661.
[9] A. Van Der Putten, A. Elzing, W. Visscher, E. Barendrecht, J. Electroanal. Chem. 205 (1986) 233–244.
[10] M.C. Román-Martínez, D. Cazorla-Amorós, A. Linares-Solano, C. Salinas-Martínez, H. Yamashita, M. Anpo, Carbon 33 (1995) 3–13.
[11] Z. Xu, Z. Qi, A. Kaufman, Electrochem. Solid State Lett. 8 (2005) A313–A315.
[12] Z. Xu, Z. Qi, A. Kaufman, Electrochem. Solid State Lett. 6 (2003) A171–A173.
[13] Z. Xu, Z. Qi, A. Kaufman, J. Chem. Soc., Chem. Commun. (2003) 878–879.
[14] E.B. Easton, Z. Qi, A. Kaufman, P.G. Pickup, Electrochem. Solid State Lett. 4 (2001) A59–A61.
[15] Z. Hou, B. Yi, H. Zhang, Electrochem. Solid State Lett. 6 (2003) A232–A235.
[16] F. Jaouen, S. Marcotte, J.-P. Dodelet, G. Lindbergh, J. Phys. Chem. B 107 (2003) 1376–1386.
[17] P. Ehrburger, A. Mongilardi, J.J. Lahaye, J. Colloid Interface Sci. 91 (1983) 151–159.
[18] P. Gouérec, M. Savy, J. Riga, Electrochim. Acta 43 (1998) 743–753.
[19] O. Contamin, C. Debiemme-Chouvy, M. Savy, G. Scarbeck, Electrochim. Acta 45 (1999) 721–729.
[20] S.A. Campbell, US Patent 0096728 A1 (2004).
[21] G. Faubert, R. Côté, J.-P. Dodelet, M. Lefèvre, P. Bertrand, M. Savy, G. Scarbeck, Electrochim. Acta 44 (1999) 2589–2603.
[22] C.F. Bell, Principles and Applications of Metal Chelation, Oxford University Press, Great Britain, 1977, p. 2.
[23] O. Ozturk, T.J. Black, K. Perrine, K. Pizzolato, J.S. Ratliff, F.W. Parsons, C.T. Williams, J. Gao, C.J. Murphy, H. Xie, H.J. Ploehn, D.A. Chen, Langmuir 21 (2005) 3998–4006.
[24] K. Kinoshita, J.A.S. Bett, Carbon 11 (1973) 403–411.
[25] H. Wang, R. Côté, G. Faubert, D. Guay, J.P. Dodelet, J. Phys. Chem. B 103 (1999) 2042–2049.
[26] R. Jiang, F.C. Anson, J. Electroanal. Chem. 305 (1991) 171–184.
[27] A.L. Bouwkamp-Wijnoltz, W. Visscher, J.A.R. van Veen, Electrochim. Acta 43 (1998) 3141–3152.
[28] K. Kinoshita, Carbon: Electrochemical and Physicochemical Properties, Wiley–Interscience, USA, 1988, p. 90.
[29] J.B. Donnet, Carbon 6 (1968) 161–176.
[30] J.E. Mark, B. Erman, F.R. Elrich, Science and Technology of Rubber, second ed., Academic Press, USA, 1994, p. 388.
[31] S. Biniak, M. Walczyk, G.S. Szymański, Fuel Process. Tech. 79 (2002) 251–257.
[32] J.-W. Shim, S.-J. Park, S.-K. Ryu, Carbon 39 (2001) 1635–1642.
[33] R.R. Witherspoon, US Patent 5240893 (1993).
[34] M. Lefèvre, J.-P. Dodelet, Electrochim. Acta 48 (2003) 2749–2760.
[35] C.D. Wagner, W.M. Riggs, L.E. Davis, J.F. Moulder, Handbook of X-Ray Photoelectron Spectroscopy: A Reference Book of Standard Data for Use in X-Ray Photoelectron Spectroscopy, Perkin-Elmer Corporation, Eden Prairie, MN, 1978.
[36] G. Faubert, R. Côté, D. Guay, J.-P. Dodelet, G. Dénès, C. Poleunis, P. Bertrand, Electrochim. Acta 43 (1998) 1969–1984.
[37] P. Gouérec, A. Biloul, O. Contamin, G. Scarbeck, M. Savy, J. Riga, L.T. Weng, P. Bertrand, J. Electroanal. Chem. 422 (1997) 61–75.